Graphitic Carbon Nitride Materials for Photocatalytic Hydrogen Production via Water Splitting: A Short Review

Seong Jun Mun and Soo-Jin Park *

Department of Chemistry, Inha University, 100 Inharo, Incheon 22212, Korea; dajoasj@gmail.com
* Correspondence: sjpark@inha.ac.kr; Tel.: +82-32-876-7234

Abstract: The generation of photocatalytic hydrogen via water splitting under light irradiation is attracting much attention as an alternative to solve such problems as global warming and to increase interest in clean energy. However, due to the low efficiency and selectivity of photocatalytic hydrogen production under solar energy, a major challenge persists to improve the performance of photocatalytic hydrogen production through water splitting. In recent years, graphitic carbon nitride (g-C_3N_4), a non-metal photocatalyst, has emerged as an attractive material for photocatalytic hydrogen production. However, the fast recombination of photoexcited electron–hole pairs limits the rate of hydrogen evolution and various methods such as modification, heterojunctions with semiconductors, and metal and non-metal doping have been applied to solve this problem. In this review, we cover the rational design of g-C_3N_4-based photocatalysts achieved using methods such as modification, metal and non-metal doping, and heterojunctions, and we summarize recent achievements in their application as hydrogen production photocatalysts. In addition, future research and prospects of hydrogen-producing photocatalysts are also reviewed.

**Keywords:** graphitic carbon nitride; photocatalysis; H_2 generation; water splitting

1. Introduction

As interest in the fossil fuel depletion and environmental pollution has increased, the development of clean energy has also recently attracted increased attention. It is important to find new alternative energy sources because of the increased use of energy, depletion of fossil fuels, and the need for sustainable energy development [1]. Among the many alternative energy sources, hydrogen-based energy systems are considered candidates for future energy because they are nonpolluting, inexhaustible, efficient, and can provide high-quality energy services in a wide range of applications [2,3]. However, most hydrogen production processes are based on natural gas [4], coal [5], crude oil [6], or the electrolysis of water [7], and unfortunately, the application of most of these processes is limited because heat and electrical energy are required. Thus, photocatalytic hydrogen production using solar energy, a clean energy resource for the foreseeable future, is considered to be an attractive way of solving the global energy issue and environmental pollution [8,9].

The overall water splitting by a photocatalyst under sunlight irradiation enables the production of environmentally friendly molecular hydrogen and does not use fossil fuel [10]. A photocatalytic system should consider the following prerequisites. First, to absorb as many photons as possible, the photocatalyst must have a narrow band-gap; to generate hydrogen from water splitting, the bottom of the conduction band (CB) must be more negative than the reduction potential of H^+/H_2 and the top of the valence band (VB) must be more positive than the oxidation potential of H_2O/O_2 [11]. Second, efficient charge separation and fast charge transport that simultaneously avoid bulk and surface charge

recombination are essential to transfer the photogenerated charge to the surface reaction site [12]. Third, because the charge carriers at the interface lack the capacity to boost the transportation process, the charge carriers mostly move via a random path and require a surface chemical reaction that is active between the charge carrier and the water or other molecules [13]. A variety of semiconductor materials such as TiO_2, ZnO, CdS, and WO_3 have been extensively studied for hydrogen generation via photocatalytic water splitting [14–17]. Among them, WO_3 absorbs visible light but has a problem in that the CB is not useful for hydrogen production because it is lower than the H reduction potential [18,19]. In addition, hydrogen evolution through photocatalytic water splitting has been extensively studied for metal oxides, quantum dots, and metal–organic frameworks, etc. However, some methods are difficult to use due to their low efficiency under visible light and the fast recombination rate of the electron–hole pairs [20–25]. Therefore, it is a major challenge to develop photocatalysts that exhibit stable water-splitting performance under visible-light irradiation for the efficient use of solar energy.

Recently, graphitic carbon nitride (g-C_3N_4) has attracted attention as a hydrogen-generating photocatalyst via water splitting. g-C_3N_4 is synthesized by the thermal condensation of nitrogen-rich precursors with a tri-s-triazine ring structure such as cyanamide, dicyandiamide, urea, or thiourea, resulting in a graphene-like structure after exfoliation (Figure 1) [26]. In addition, it has a band gap of ~2.7 eV corresponding to 460 nm in the visible range and high thermal and chemical stability [27].
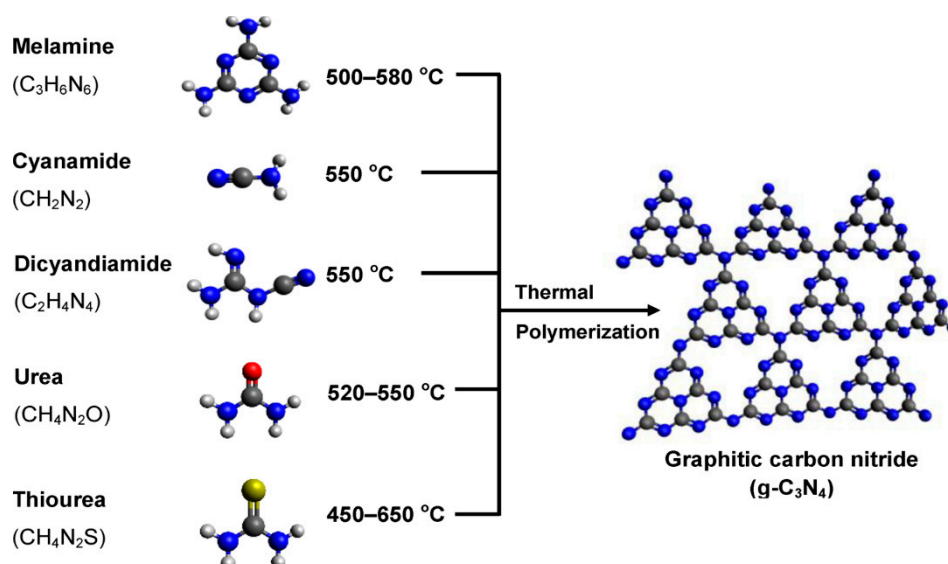
Figure 1. Schematic illustration of the synthesis process from the possible precursors of g-C_3N_4. Reproduced with permission from [26]; copyright (2016), the American Chemical Society.

However, there are some drawbacks to using g-C_3N_4 as a water-splitting photocatalyst. The relatively large band-gap and low charge-carrier mobility limit the electron and hole separation and transport and thus limit the effective use of visible light [28]. Thus, increasing hydrogen production during photocatalytic water splitting under visible-light irradiation is necessary through a variety of methods such as creating heterojunctions with semiconductors and doping with other elements [29–33]. As a result, the focus of this review is on summarizing the current and prospective advances in photocatalysis research based on g-C_3N_4 that make it effective even under visible-light irradiation.

2. The Principles of H_2 Generation via Water Splitting

Photocatalytic reactions can be divided into three parts. The first step is to obtain photons with energies that exceed the photocatalyst's band gap of the electron–hole pairs, the second step is the separation of the carrier in the photocatalyst by transfer, and the third step is the reaction between the carrier and H_2O. In addition, the electron–hole pairs are concurrently combined with each other.

The photocatalyst is involved in the production of hydrogen, but the lowest position of the CB should be lower than the reduction position of H_2O/H_2 and the position of the VB should be higher than the potential of H_2O/O_2 [34–40].

Figure 2 shows the band gap and band edge positions of various semiconductor photocatalysts [41]. A variety of these, such as ZnO, TiO_2, and WO_3 have been studied for solar hydrogen production and degradation of organic pollutants [42–45]. However, although there are exceptions for some semiconductor photocatalysts, most of the semiconductor photocatalysts have low efficiency under visible-light irradiation. Therefore, it is a major challenge to develop photocatalysts that efficiently exploit solar energy.
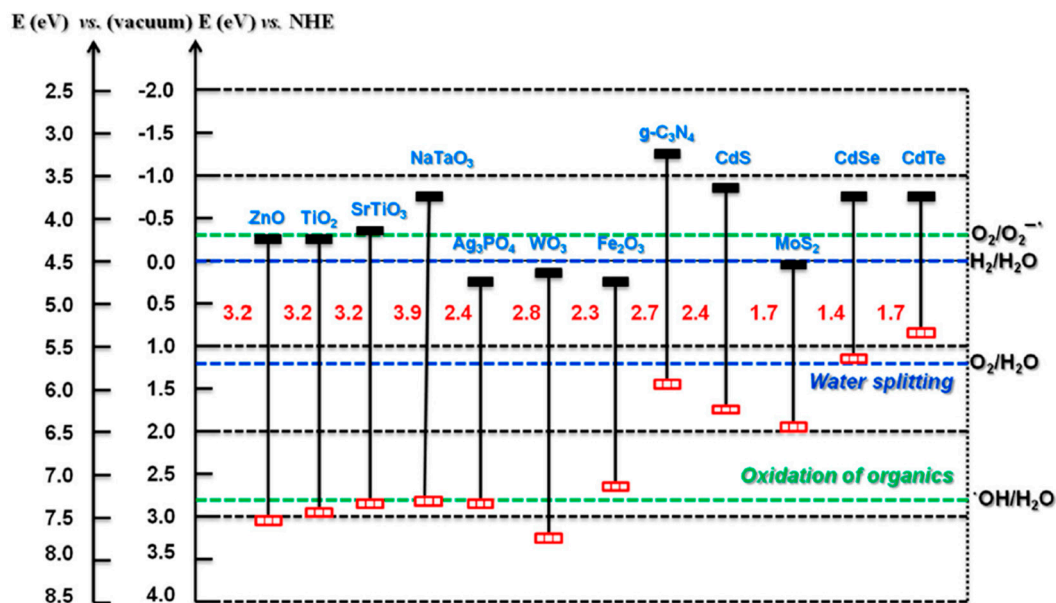
Figure 2. A schematic illustration of the band-gap energy of several typical semiconductor photocatalysts. Reproduced with permission from [41].

Recently, g-C_3N_4, which has a unique electron band structure for photo-oxidation and reduction, has been confirmed by several researchers as an efficient photocatalyst for visible-light activation for photochemical reactions [46]. This achieves the photoexcited state when creating electron–hole pairs where photogenerated electrons are involved in the reduction process while the holes are consumed in the oxidation process [47]. The excited electrons and holes act as reactive species that are highly oxidizing and reducing. The excited electrons and holes travel to the active sites on the surface, thereby splitting the water into oxygen and hydrogen (Figure 3) [48]. However, despite its excellent electron and optical properties, g-C_3N_4 has low efficiency for visible-light utilization and a high recombination speed of photoelectric carrier, resulting in the poor formation of radical species causing redox reaction during the photocatalytic reaction [49]. It has a low specific surface area, provides fewer reactive sites, and reduces light harvesting. In addition, the low bandgap (2.7 eV) of g-C_3N_4 is still quite large for efficient visible-light harvesting and has limited use, leaving much of the visible-light spectrum unexploited.
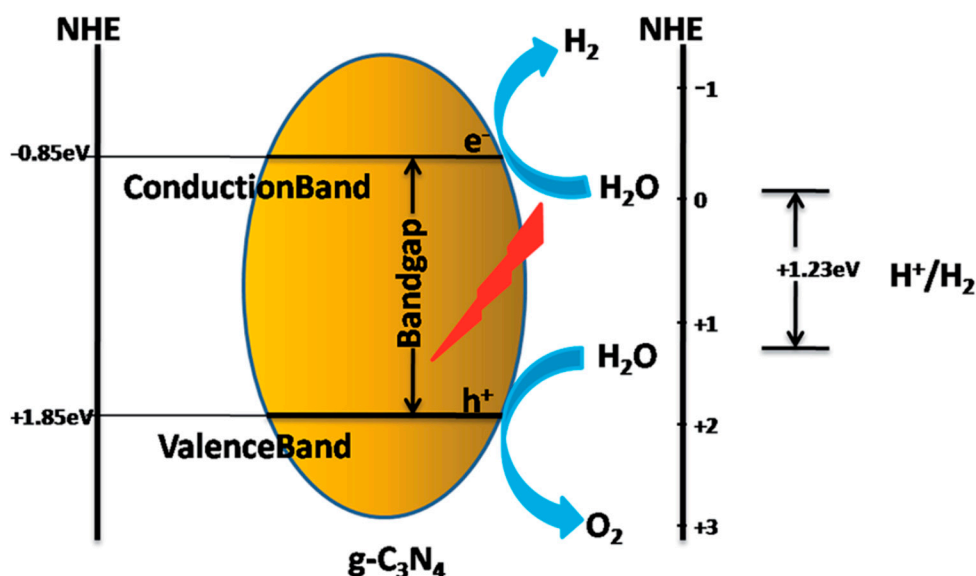
Figure 3. Schematic illustration of the charge-transfer mechanism of neat g-C$_3$N$_4$ as a photocatalyst. Reproduced with permission from [48]; copyright (2016), Royal Society of Chemistry Advances.

## 3. Hydrogen Generation of g-C$_3$N$_4$-Based Photocatalysts

In recent years, a review of the technological improvements of the photocatalytic efficiency of g-C$_3$N$_4$-based materials has been published, mostly focusing on contaminant removal, the reaction mechanisms, principles of photocatalysis, and the effects of operational parameters [50,51]. Therefore, the aim of this review is to summarize recent trends in the improvement of hydrogen production by photocatalysts using various methods for the purpose of improving g-C$_3$N$_4$-based photocatalytic hydrogen production: (1) modification of g-C$_3$N$_4$; (2) heterojunctions from g-C$_3$N$_4$/semiconductors; and (3) metal- and non-metal-doped g-C$_3$N$_4$.

3.1. Modification of g-C$_3$N$_4$

Improving the photocatalytic activity of g-C$_3$N$_4$ by introducing various nanostructures such as nanoparticles, nanosheets, nanorods, and nanowires has recently been studied [52–56]. Surface modification of the catalytic structure and morphology has the potential to promote charge separation and narrow the band gap due to increased surface area and efficient charge-carrier separation [57,58].

In 2016, Han et al. [59] reported an atomically thin mesoporous nanomesh of g-C$_3$N$_4$ for hydrogen evolution by highly efficient photocatalysts (Figure 4a) fabricated via the solvothermal exfoliation of mesoporous g-C$_3$N$_4$ prepared by the thermal polymerization of freeze-dried nanostructured precursors. The delamination of the layer material to provide the two-dimensional single-atom sheet has led to unique physical properties such as a large surface area, a very high unique carrier mobility, and a significant change in the energy band structure [60]. The mesoporous g-C$_3$N$_4$ nanomesh shows inherent structural advantages, electron transfer capability, and efficient light harvesting. Figure 4b shows the electronic band structure of the monolayer mesoporous g-C$_3$N$_4$ nanomesh and bulk counterparts. The band gap is 2.75 eV for the monolayer mesoporous g-C$_3$N$_4$ nanomesh and 2.59 eV for the bulk counterpart, as determined from optical absorption spectra. The VB of the monolayer mesoporous g-C$_3$N$_4$ nanomesh (2.41 eV) identified via X-ray photoelectron spectroscopy is also 0.35 eV higher than the bulk counterparts (2.06 eV). The CB is upshifted by 0.51 eV when considering the 0.16 eV increase in the VB and a negative shift of 0.35 eV. The monolayer mesoporous g-C$_3$N$_4$ nanomesh exhibits significantly improved the light-harvesting ability mainly due to the multiple scattering effect and the presence of defect sites associated with the mesoporous surface. A 30 h reaction was performed with intermittent evacuation every 5 h to confirm the hydrogen production ability of mesoporous g-C$_3$N$_4$

nanomesh under visible-light irradiation (Figure 4c). As a result, the 2.6 mmol H_2 gas (59 mL) produced by the atomically thin mesoporous g-C_3N_4 nanomesh was not visibly deactivated and the H_2 gas was generated continuously. Wavelength-dependent H_2 evolution shows the optical absorption spectrum of monolayer g-C_3N_4 nanomesh, indicating that the H_2 generation is driven by photoinduced electrons in g-C_3N_4 (Figure 4d). In conclusion, the mesoporous g-C_3N_4 nanomesh produces an atomically thin mesoporous layer during the freeze-dried assembly and solvothermal exfoliation. Its good application benefits from structural advantages for light harvesting, electron transport, and accessible reaction sites [61]. This new type of mesoporous g-C_3N_4 nanomesh could be applied to photocatalytic and various engineering fields.
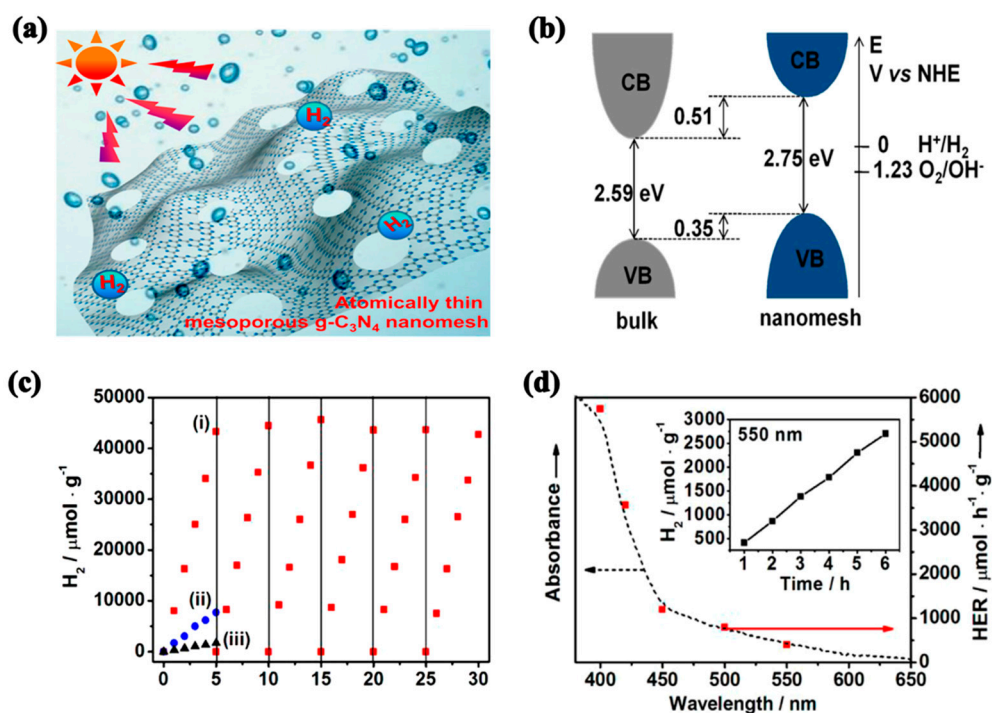

Figure 4. (**a**) Schematic illustration of atomically thin mesoporous g-C_3N_4 nanomesh photocatalyst and (**b**) a band gap schematic of the monolayer mesoporous g-C_3N_4 nanomesh and bulk counterparts. (**c**) Hydrogen production rate of the monolayer mesoporous g-C_3N_4 nanomesh, the bulk counterpart, and the traditional g-C_3N_4 bulk under visible-light irradiation. (**d**) H_2 evolution rate on the monolayer mesoporous g-C_3N_4 nanomesh with wavelength dependence. Reproduced with permission from [59]; copyright (2016), American Chemical Society.

In 2018, Zhao et al. [62] reported the fabrication of a mesoporous g-C_3N_4 consisting of hollow nanospheres (MCNHN) via a simple vapor-deposition method that improved hydrogen production under visible-light irradiation. Figure 5a shows the photocatalytic hydrogen evolution by MCNHN under visible-light irradiation. Both MCNHN and bulk g-C_3N_4 achieved a stable average rate of hydrogen production within 4 h, but the hydrogen evolution of MCNHN was 659.8 μmol g^{-1} h^{-1}, which is 22.3 times greater than bulk g-C_3N_4 (29.6 μmol g^{-1} h^{-1}). The excellent hydrogen production activity of MCNHN is due to its well-defined structure. The increased surface area provides more active sites in the photocatalytic reaction, thereby allowing more light to be harvested. Moreover, the planarized unit layer and the decreased interlayer space of g-C_3N_4 crystals facilitate the transfer and separation of photoinduced charge carriers in MCNHN. As a result, photocatalytic hydrogen generation is significantly improved due to the large surface area and decreased interlayer space of g-C_3N_4. Figure 5b shows the proposed photocatalytic mechanism of H_2 evolution for MCNHN based on the aforementioned results and the literature. The active site of MCNHN absorbs visible

light. Electrons in the VB are excited to the CB by absorption of photons, and are then transferred to the Pt nanoparticles loaded on the surface of MCNHN; the corresponding photoexcited holes remain in the VB. The electron-rich Pt nanoparticles become active sites where water can be split into hydrogen. In addition, multiple reflections of visible light in the MCNHN with Pt nanoparticles improves light absorption.
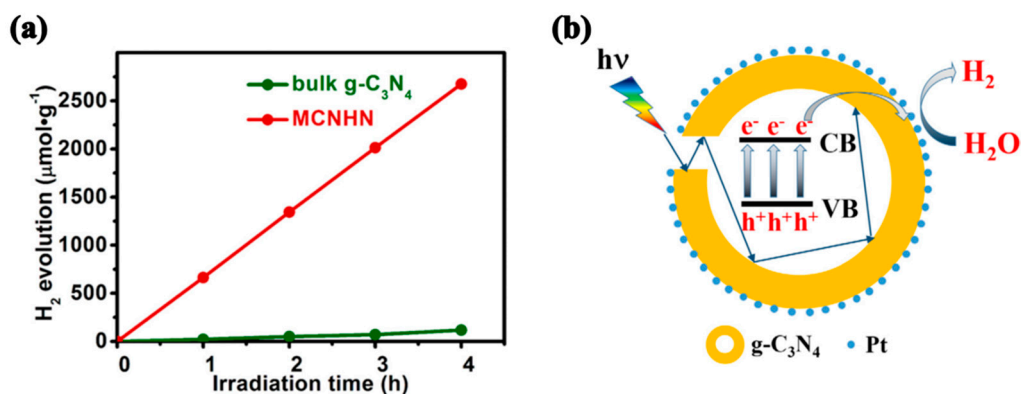
Figure 5. (**a**) Time course of H_2 evolution and (**b**) a schematic mechanism for photocatalytic H_2 evolution on MCNHN. Reproduced with permission from [62]; copyright (2018), Elsevier.

3.2. Heterojunctions and Photocatalysis

Electron–hole charge pairs formed by the photocatalytic hydrogen evolution reaction are transferred to the surface of the photocatalyst or else recombine with each other. To better understand this point, let us illustrate it by reviewing the presentation in [63]: a comparison of the influence of gravitational force on a man jumping off the ground and electrons jumping from the VB to the CB (Figure 6a,b, respectively). If a man (electron) jumps from the ground (VB) into the sky (CB), it will return to the floor quickly (recombine with the hole) due to gravitational force. However, a stool (semiconductor B) can be provided to get the man off the ground (separate the photogenerated electron–hole pair), as illustrated in Figure 6c,d, respectively. Subsequently, the aforementioned man will land again on the stool rather than the ground (the electron–hole pair recombination will be inhibited). Preventing electron–hole recombination is an urgent issue, but it can be achieved by the proper design of materials [64–66]. Many methods have been proposed to achieve better separation of the photogenerated electron–hole pairs in semiconductor photocatalysts, such as element combining, metal and non-metal doping, and heterojunctions [67–72]. Among these strategies, heterojunctions in photocatalysts have proved to be one of the most promising methods for efficient photocatalyst preparation due to their improved separation of electron–hole pairs [73].
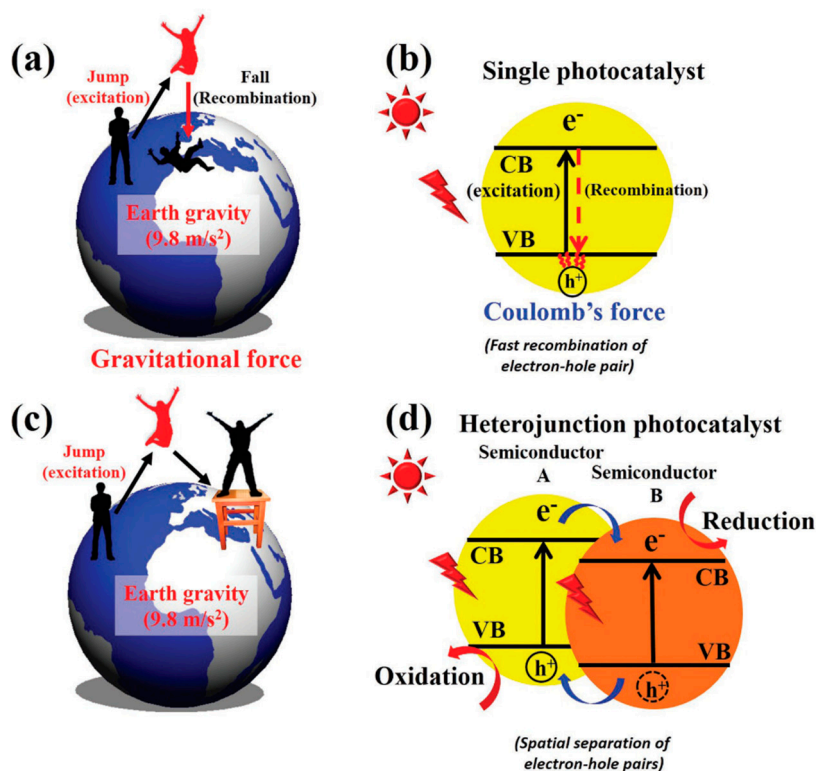
Figure 6. Schematics of (**a**) the influence of gravitational force on a man jumping; (**b**) recombination of photocatalyst electron–hole pair; (**c**) using stool to keep a man from returning to the ground; and (**d**) electron–hole pairs separated in a heterojunction photocatalyst. Reproduced with permission from [63]; copyright (2017), John Wiley & Sons, Inc.

3.2.1. Semiconductor Heterojunction Photocatalysts

Suppressing the electron–hole recombination rate is the most important solution to increase photocatalytic efficiency. Bulk g-C_3N_4 has low ability to collect visible light, low charge-transport properties, and small surface area, so there have been many studies to make it an efficient photocatalyst [74]. Various strategies have been proposed to achieve better electron–hole pair separation such as element combining, metal doping, and creating heterojunctions. Among these strategies, g-C_3N_4/semiconductor heterojunctions have shown the improved separation capability of electron–hole pairs; the charge carrier is transferred through the heterostructure interface to inhibit recombination, thereby improving the photocatalytic performance [75–77]. In addition, a g-C_3N_4/semiconductor heterostructure can be formed by combining a visible-light excited photocatalyst semiconductor material having a narrow band-gap and a photoexcited photocatalyst having a large band-gap in a coupling process; the connection between the two different kinds of photocatalyst having different band structures induces a new band arrangement [78,79].

In 2017, Zhang et al. [80] reported the in situ synthesis of a g-C_3N_4/TiO_2 heterostructure photocatalyst which greatly improved the hydrogen evolution performance under visible light. The g-C_3N_4 nanosheets were synthesized by calcining urea at 550 °C for 4 h. Two hundred milligrams of the as-prepared g-C_3N_4 nanosheets were dispersed in 20 mL ethanol and sonicated for 1 hour to obtain a homogeneous suspension. Under continuous stirring, 40 mL of ammonia solution (~28 wt%) and tetrabutyl titanate (TBT) (0, 100, 200, 300 and 400 μL) were added and stirred for 12 h to achieve the in situ synthesis of amorphous TiO_2. The obtained products were expressed as CNTO-*x* (*x* = 0–4) according to the TBT content. As shown in Figure 7a, the shape of the CNTO-2 sample seen in a transmission electron microscopy (TEM) image shows that the TiO_2 nanoparticles are uniformly distributed in the g-C_3N_4 nanosheets. As a result, there is uniform interfacial contact between the

TiO_2 phase and the g-C_3N_4 phase. Figure 7b shows the average rate of hydrogen production within 3 h. Pure TiO_2 does not react with visible light and produces negligible H_2, while CNTO-0 exhibits a low hydrogen production rate of 15 μmol h^{-1} due to the fast recombination of photogenerated charge carriers. In contrast, the CNTO-2 sample exhibits significantly improved hydrogen production performance at 40 μmol h^{-1}. However, as the amount of TiO_2 is further increased, TiO_2 occupies the surface of g-C_3N_4 resulting in less active sites for H_2 evolution. The proposed mechanism of heterostructure composites is also shown in Figure 7c. According to previous reports, the CB and VB potentials of g-C_3N_4 and TiO_2 are -1.12 and $+1.58$ V, and -0.29 and $+2.91$ V, respectively. Under visible light irradiation, only g-C_3N_4 can absorb light to generate electron–hole pairs. However, in pure g-C_3N_4, photogenerated electrons and holes recombine rapidly, and only a few of the electrons participate in the reaction, resulting in low reactivity. When g-C_3N_4 is modified by TiO_2 to form a heterojunction structure, the CB edge of g-C_3N_4 is more negative than TiO_2, so that electrons excited in the CB of g-C_3N_4 can be injected directly into the CB of TiO_2. Consequently, Pt^{2+} adsorbed on the surface is reduced by electrons transferred from the CB of TiO_2, and newly formed Pt nanoparticles are deposited on the surface of TiO_2 as an efficient cocatalyst for hydrogen production. The electrons then accumulate in Pt nanoparticles and participate in hydrogen evolution. Therefore, the photocatalytic activity of the g-C_3N_4/TiO_2 composite with Pt nanoparticles as a cocatalyst is significantly improved.
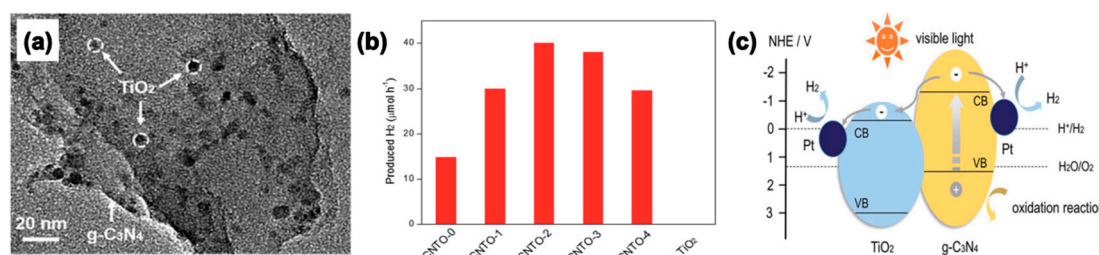

Figure 7. (**a**) A TEM image of CNTO-2, (**b**) H_2 evolution rates of the CNTO-*x* samples under visible light ($\lambda \geq 420$ nm), and (**c**) an illustration of the g-C_3N_4/TiO_2 heterojunction system. Reproduced with permission from [80]; copyright (2017), The Royal Society of Chemistry.

3.2.2. Z-Scheme Heterojunction Photocatalysts

In 2017, Lu et al. [81] reported a Z-scheme photocatalyst that improved the photocatalytic hydrogen production of g-C_3N_4 nanosheets by loading porous silicon (PSi). The Z-scheme heterostructure improved the photocatalytic H_2 evolution performance by loading PSi onto the g-C_3N_4 photocatalyst. g-C_3N_4/PSi composites were prepared by the facile polycondensation reaction of PSi with urea at various PSi content ratios and included pure g-C_3N_4 that was not PSi loaded for comparison. The photocatalytic performance of the g-C_3N_4/PSi composites and pure g-C_3N_4 in Figure 8a was evaluated by H_2 evolution from water under visible-light irradiation. For composite materials loaded with PSi on g-C_3N_4 nanosheets, the rate of H_2 evolution was better than that of pure g-C_3N_4 (427.28 μmol g^{-1} h^{-1}). In particular, the g-C_3N_4/2.50 wt% composite exhibited the highest photocatalytic activity with a hydrogen evolution rate of 870.58 μmol g^{-1} h^{-1}, which is around twice as high as that of pure g-C_3N_4. However, in the case of the Si-based photocatalyst, a passive oxide film was formed on the Si surface, and thus the stability suffered. When the PSi content was larger than 2.50 wt%, the H_2 generation activity was reduced. Figure 8b depicts an energy band diagram of g-C_3N_4/PSi with the redox potential of the photocatalytic reaction. The Z-scheme heterostructure system is recognized as the photocatalytic mechanism for the g-C_3N_4/PSi composite, and the electrons excited from the CB of PSi in the photocatalyst system can be transferred to the VB of g-C_3N_4. In addition, the holes generated in g-C_3N_4 can move to the CB of PSi through the interface formed between g-C_3N_4 and PSi. The recombination at the interface between the electrons and the holes accumulates a large number of bonds and acts as a recombination center for the electron–hole pairs [82,83]. As a result, the efficiency

of the photogenerated electron–hole pairs is improved, thereby improving photocatalytic hydrogen production under visible-light irradiation.
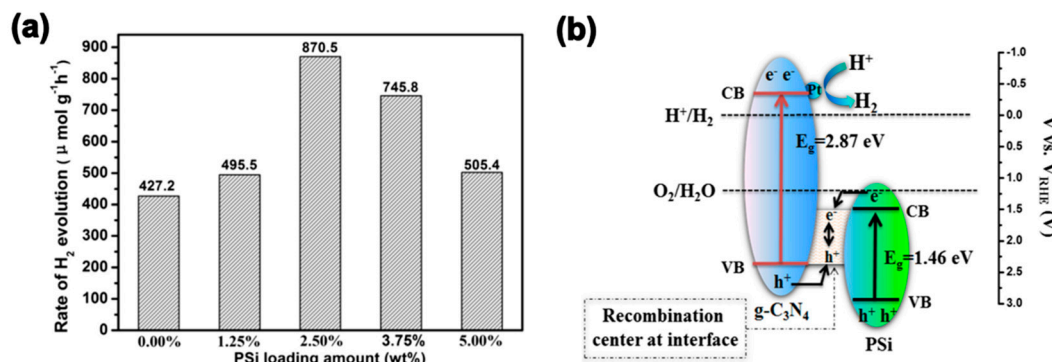

Figure 8. (**a**) Photocatalytic H_2 evolution with 100 mg pure g-C_3N_4 and g-C_3N_4/PSi composite photocatalysts under visible light (400 nm) and (**b**) a schematic diagram of the g-C_3N_4/TiO_2 heterojunction system. Reproduced with permission from [81]; copyright (2017), Elsevier.

3.3. Metal- and Non-Metal-Doped g-C_3N_4

Among the strategies for making g-C_3N_4 as a photocatalyst capable of effective hydrogen production, sufficient doping with metallic and nonmetallic elements is known to enhance the photocatalytic activity of g-C_3N_4. Metal doping is an effective strategy to adjust the electronic structure of g-C_3N_4 and promotes surface kinetics to accelerate photogenerated electron transfer and provide active sites for better photocatalytic hydrogen production. In addition, the light transmittance can be maximized since the spatial distribution and the particle size of the metal can be finely controlled to provide a sufficient active size.

In 2016, Li et al. [84] reported water splitting by Cu- and Fe-doped g-C_3N_4 visible-light-activated photocatalysts. Figure 9a shows the mechanism of water splitting by light-driven catalysis with Fe- and Cu-doped g-C_3N_4. Under visible-light irradiation, water is converted to H_2 and H_2O_2, and then H_2O_2 is further converted to O_2 and H_2O via the photocatalytic imbalance path. After absorbing visible light, g-C_3N_4 forms excited electrons and holes by electron catalysis, and the electrons move from the energy potential difference between g-C_3N_4 and Fe or Cu to the metal Fe or Cu sites. The potential of these electrons is around −0.25 eV and has enough force to induce H_2O_2 disproportionation to form ·OH and OH^-. In the hole catalytic process (HCP), OH^- and H_2O_2 could form the ·O_2^- and H_2O species reaction with the holes. Finally, O_2^- and OH can recombine to form O_2. Electron catalysis is an energy-consuming process whereas HCP and recombination processes can be viewed as energy-releasing processes. Figure 9b shows the oxygen and hydrogen evolution rates of Fe/C_3N_4 (0.37 wt%) and Cu/C_3N_4 (0.42 wt%) under visible-light irradiation ($\lambda \geq 420$ nm) for 12 h. In this case, the production of hydrogen and oxygen by the Cu/C_3N_4 and Fe/C_3N_4 photocatalysts were 1.4 and 0.5 μmol, and 2.1 and 0.8 μmol, respectively. In addition, the potential of the Fe/g-C_3N_4 photocatalyst is obviously lower than those of the g-C_3N_4 and Cu/g-C_3N_4 photocatalysts, which leads to the O_2 and H_2 evolution activity over the Fe/g-C_3N_4 photocatalyst being clearly higher than that over the g-C_3N_4 and Cu/g-C_3N_4 photocatalysts. The findings of this study give new insight into the designing of efficient catalysts for overall water splitting.
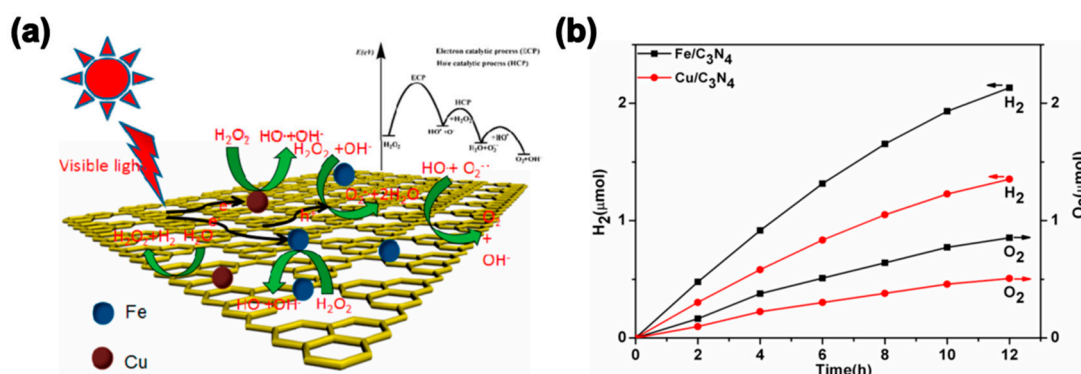
Figure 9. (**a**) A schematic diagram of the water splitting mechanism by Fe/C_3N_4 and Cu/C_3N_4 photocatalysts under visible-light irradiation. (**b**) Production of H_2 and O_2 by water splitting by the Fe/C_3N_4 and Cu/C_3N_4 photocatalysts under visible-light irradiation for 12 h. Reproduced with permission from [84]; copyright (2015), American Chemical Society.

Non-metal doping is a useful strategy to adjust the electronic structure of g-C_3N_4 and to increase the photocatalytic effect by promoting the reaction surface. When the non-metal elements B, N, O, P, and S are used to dope g-C_3N_4, the photocatalyst is efficiently optimized by lowering the charge recombination rate due to optical absorption and accelerated charge mobility, and thus the amount of H_2 produced can be increased [85,86]. Consequently, the potential of the Fe/g-C_3N_4 photocatalyst is obviously lower than those of the g-C_3N_4 and Cu/g-C_3N_4 photocatalysts. This indicates that the Fe/g-C_3N_4 photocatalyst has higher activity on photocatalytic hydrogen evolution than the g-C_3N_4 and Cu/g-C_3N_4 photocatalysts. The findings of this study give new insights into designing efficient photocatalytic hydrogen generation and catalysts through overall water splitting.

In 2018, Feng et al. [87] reported P nanostructures with P-doped g-C_3N_4 as light photocatalysts for H_2 evolution. P nanostructures and P-doped g-C_3N_4 (P@P-g-C_3N_4) were synthesized via a solid reaction, and P@P-g-C_3N_4 showed increased optical absorption, high-efficiency transmission, and efficient separation of photogenerated electron–hole pairs. When C atoms are replaced with P atoms (the gray and red balls in Figure 10a, respectively) in the base frame of g-C_3N_4, the extra electrons are decentralized into a π-conjugated triazine ring and generate a positive-charge P^+ center, thereby facilitating rapid separation of the photogenerated excited electrons. Furthermore, efficient band gap transfers between the P and P-doped g-C_3N_4 leads to a significant improvement in photoactivity (Figure 10b). P-doped g-C_3N_4 photoexcited electrons can be delivered to phosphorus via intimate contact because the CB edge of g-C_3N_4 (-1.2 V vs. normal hydrogen electrode (NHE)) is more negative than P (-0.25 V vs. NHE) which provides an interface under the buildup of the internal electric field. Thus, the extra electrons superimposed on the P surface can easily be captured by the oxygen molecules in the solution and react with $\cdot O^{2-}$ and $\cdot OH$. Figure 10c,d shows the hydrogen evolution yield and the improvement in hydrogen production ability of the photocatalysts prepared at different weight ratios of P/g-C_3N_4. P@P-g-C_3N_4-15 showed the highest hydrogen production rate (941.80 $\mu mol\ h^{-1}\ g^{-1}$), which is around four times that of conventional g-C_3N_4.
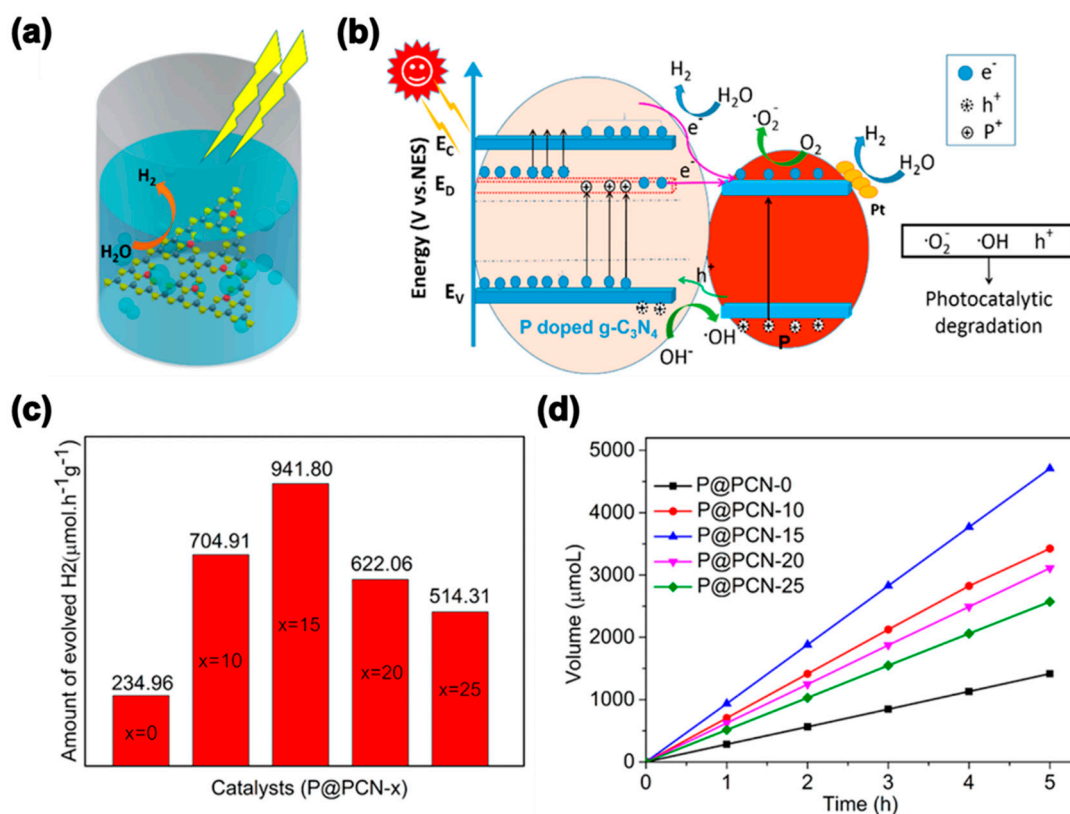
Figure 10. (**a**,**b**) A schematic of the mechanism of H_2 evolution by the P@P-g-C_3N_4 catalyst; (**c**) comparison of the evolution rates of H_2; and (**d**) H_2 evolution rate of the P@P-g-C_3N_4 composites. Reproduced with permission from [87]; copyright (2018), American Chemical Society.

4. Summary and Perspectives

Photocatalytic action is a key factor for the future of environmental pollution and hydrogen generation due to water splitting. Over the past several years, photocatalytic reactions have emerged as a promising method to generate hydrogen, and interest in the photocatalyst g-C_3N_4 has received attention in a variety of scientific disciplines. However, a major problem that limits the rate of production of H_2 by g-C_3N_4-based photocatalysis is the fast recombination of photoexcited electron–hole pairs. This problem can be solved in a variety of ways, including modification, heterojunctions, and metal and non-metal doping. Table 1 summarizes the literature on the photocatalytic H_2 generation of g-C_3N_4-based materials. We reviewed the rational design of photocatalysts for efficient H_2 generation though a variety of methods. Furthermore, the improvement of g-C_3N_4-based photocatalysts will likely result from advances in science. Herein, we have covered the recent progress of g-C_3N_4-based materials involved in hydrogen production in improving their overall photocatalytic activity and have characterized their performance and importance. We hope that this report will support further research efforts related to photocatalytic development.

Table 1. Photocatalytic H_2 generation of g-C_3N_4-based materials.

Entry	Type	Mass Fraction of g-C_3N_4	Mass of Photocatalyst	Reactant Solution	Light Source	H_2 Generation Rate (μmol h^{-1})	Reference
Figure 4	Monolayer mesoporous g-C_3N_4 nanomesh	100 wt%	0.01 g	100 mL of 10 vol% triethanolamine aqueous solution; 3 wt% Pt as a cocatalyst	300 W Xe lamp (>420 nm)	85.10	[59]
Figure 5	Mesoporous g-C_3N_4 comprising hollow nanospheres	100 wt%	0.1 g	100 mL of 10 vol.% triethanolamine aqueous solution; 3 wt% Pt as a cocatalyst	300 W Xe lamp (>420 nm)	65.98	[62]
Figure 7	g-C_3N_4 nanosheets/TiO$_2$	50 wt%	0.05 g	100 mL of 10 vol% triethanolamine aqueous solution; 3 wt.% Pt as a cocatalyst	300 W Xe lamp (>420 nm)	40	[80]
Figure 8	Porous Si-loaded g-C_3N_4	97.50 wt%	0.1 g	100 mL of 10 vol% triethanolamine aqueous solution; 3 wt% Pt as a cocatalyst	300 W Xe lamp (>400 nm)	87.05	[81]
Figure 9	Fe-doped g-C_3N_4 Cu-doped g-C_3N_4	99.63 wt% 99.58 wt%	0.01 g	Pure water; without other cocatalyst	300 W Xe lamp (>420 nm)	0.175	[84]
Figure 10	P@P-doped g-C_3N_4	75 wt%	0.1 g	100 mL of 10 vol% triethanolamine aqueous solution; 1 wt% Pt as a cocatalyst	300 W Xe lamp (>420 nm)	94.18	[87]

Conflicts of Interest: The authors declare no conflict of interest.

References

1. Armaroli, N.; Balzani, V. The future of energy supply: Challenges and opportunities. *Chem.-Int. Ed.* **2007**, *46*, 52–66. [CrossRef] [PubMed]
2. Kudo, A.; Miseki, Y. Heterogeneous photocatalyst materials for water splitting. *Chem. Soc. Rev.* **2009**, *38*, 253–278. [CrossRef] [PubMed]
3. Zhou, H.; Fan, T.; Zhang, D. Biotemplated materials for sustainable energy and environment: Current status and challenges. *ChemSusChem* **2011**, *4*, 1344–1387. [CrossRef] [PubMed]
4. Dicks, A.L. Hydrogen generation from natural gas for the fuel cell systems of tomorrow. *J. Power Sources* **1996**, *61*, 113–124. [CrossRef]
5. Lin, S.; Harada, M.; Suzuki, Y.; Hatano, H. Hydrogen production from coal by separating carbon dioxide during gasification. *Fuel* **2002**, *81*, 2079–2085. [CrossRef]
6. Rana, M.S.; Sámano, V.; Ancheyta, J.; Diaz, J.A.I. A review of recent advances on process technologies for upgrading of heavy oils and residua. *Fuel* **2007**, *86*, 1216–1231. [CrossRef]
7. Zeng, K.; Zhang, D. Recent progress in alkaline water electrolysis for hydrogen production and applications. *Prog. Energy Combust. Sci.* **2010**, *36*, 307–326. [CrossRef]
8. Acar, C.; Dincer, I.; Naterer, G.F. Review of photocatalytic water-splitting methods for sustainable hydrogen production. *Int. J. Energy Res.* **2016**, *40*, 1449–1473. [CrossRef]
9. Tong, H.; Ouyang, S.; Bi, Y.; Umezawa, N.; Oshikiri, M.; Ye, J. Nano-photocatalytic materials: Possibilities and challenges. *Adv. Mater.* **2012**, *24*, 229–251. [CrossRef]
10. Lubitz, W.; Tumas, W. Hydrogen: An overview. *Chem. Rev.* **2007**, *107*, 3900–3903. [CrossRef]
11. Christoforidis, K.C.; Fornasiero, P. Photocatalytic hydrogen production: A rift into the future energy supply. *ChemCatChem* **2017**, *9*, 1523–1544. [CrossRef]
12. Maeda, K.; Domen, K. Photocatalytic Water Splitting: Recent Progress and Future Challenges. *J. Phys. Chem. Lett.* **2010**, *1*, 2655–2661. [CrossRef]
13. Wei, P.; Liu, J.; Li, Z. Effect of Pt loading and calcination temperature on the photocatalytic hydrogen production activity of TiO_2 microspheres. *Ceram. Int.* **2013**, *39*, 5387–5391. [CrossRef]
14. Choi, S.K.; Yang, H.S.; Kim, J.H.; Park, H. Organic dye-sensitized TiO_2 as a versatile photocatalyst for solar hydrogen and environmental remediation. *Appl. Catal. B Environ.* **2012**, *121*, 206–213. [CrossRef]
15. Liu, D.; Zhang, S.; Wang, J.; Peng, T.; Li, R. Direct Z-Scheme 2D/2D Photocatalyst Based on Ultrathin g-C_3N_4 and WO_3 Nanosheets for Efficient Visible-Light-Driven H_2 Generation. *ACS Appl. Mater. Interfaces* **2019**, *11*, 27913–27923. [CrossRef] [PubMed]
16. Kudo, A. Photocatalyst materials for water splitting. *Catal. Surv. Asia* **2003**, *7*, 31–38. [CrossRef]
17. Yuan, L.; Han, C.; Yang, M.-Q.; Xu, Y.-J. Photocatalytic water splitting for solar hydrogen generation: Fundamentals and recent advancements. *Int. Rev. Phys. Chem.* **2016**, *35*, 1–36. [CrossRef]
18. Huang, L.; Xu, H.; Li, Y.; Li, H.; Cheng, X.; Xia, J.; Cai, G. Visible-light-induced WO_3/g-C_3N_4 composites with enhanced photocatalytic activity. *Dalton Trans.* **2013**, *42*, 8606–8616. [CrossRef]
19. Wang, G.; Ling, Y.; Wang, H.; Yang, X.; Wang, C.; Zhang, J.Z.; Li, Y. Hydrogen-treated WO_3 nanoflakes show enhanced photostability. *Energy Environ. Sci.* **2012**, *5*, 6180–6187. [CrossRef]
20. Wang, C.C.; Yi, X.H.; Wang, P. Powerful combination of MOFs and C_3N_4 for enhanced photocatalytic performance. *Appl. Catal. B Environ.* **2019**, *247*, 24–48. [CrossRef]
21. Pant, B.; Park, M.; Kim, H.Y.; Park, S.J. CdS-TiO_2 NPs decorated carbonized eggshell membrane for effective removal of organic pollutants: A novel strategy to use a waste material for environmental remediation. *J. Alloy. Compd.* **2017**, *699*, 73–78. [CrossRef]

22. Pullen, S.; Fei, H.; Orthaber, A.; Cohen, S.M.; Ott, S. Enhanced photochemical hydrogen production by a molecular diiron catalyst incorporated into a metal–organic framework. *J. Am. Chem. Soc.* **2013**, *135*, 16997–17003. [CrossRef]

23. Cao, S.W.; Yuan, Y.P.; Fang, J.; Shahjamali, M.M.; Boey, F.Y.; Barber, J.; Xue, C. In-situ growth of CdS quantum dots on g-C$_3$N$_4$ nanosheets for highly efficient photocatalytic hydrogen generation under visible light irradiation. *Int. J. Hydrog. Energy* **2013**, *38*, 1258–1266. [CrossRef]

24. Wang, W.; Jimmy, C.Y.; Shen, Z.; Chan, D.K.; Gu, T. g-C$_3$N$_4$ quantum dots: Direct synthesis, upconversion properties and photocatalytic application. *Chem. Commun.* **2014**, *50*, 10148–10150. [CrossRef] [PubMed]

25. Zhou, L.; Tian, Y.; Lei, J.; Wang, L.; Liu, Y.; Zhang, J. Self-modification of g-C$_3$N$_4$ with its quantum dots for enhanced photocatalytic activity. *Catal. Sci. Technol.* **2018**, *8*, 2617–2623. [CrossRef]

26. Ong, W.J.; Tan, L.L.; Ng, Y.H.; Yong, S.T.; Chai, S.P. Graphitic carbon nitride (g-C$_3$N$_4$)-based photocatalysts for artificial photosynthesis and environmental remediation: Are we a step closer to achieving sustainability? *Chem. Rev.* **2016**, *116*, 7159–7329. [CrossRef] [PubMed]

27. Naseri, A.; Samadi, M.; Pourjavadi, A.; Moshfegh, A.Z.; Ramakrishna, S. Graphitic carbon nitride (g-C$_3$N$_4$)-based photocatalysts for solar hydrogen generation: Recent advances and future development directions. *J. Mater. Chem. A* **2017**, *5*, 23406–23433. [CrossRef]

28. Liao, G.; Chen, S.; Quan, X.; Yu, H.; Zhao, H. Graphene oxide modified g-C$_3$N$_4$ hybrid with enhanced photocatalytic capability under visible light irradiation. *J. Mater. Chem.* **2012**, *22*, 2721–2726. [CrossRef]

29. Bhunia, M.K.; Yamauchi, K.; Takanabe, K. Harvesting solar light with crystalline carbon nitrides for efficient photocatalytic hydrogen evolution. *Angew. Chem. Int. Ed. Engl.* **2014**, *53*, 11001–11005. [CrossRef]

30. Hen, S.; Wang, C.; Bunes, B.R.; Li, Y.; Wang, C.; Zang, L. Enhancement of visible-light-driven photocatalytic H$_2$ evolution from water over g-C$_3$N$_4$ through combination with perylene diimide aggregates. *Appl. Catal. A Gen.* **2015**, *498*, 63–68.

31. Jiang, L.; Yuan, X.; Pan, Y.; Liang, J.; Zeng, G.; Wu, Z.; Wang, H. Doping of graphitic carbon nitride for photocatalysis: A reveiw. *Appl. Catal. B Environ.* **2017**, *217*, 388–406. [CrossRef]

32. Zhu, Y.-P.; Ren, T.-Z.; Yuan, Z.-Y. Mesoporous phosphorus-doped g-C$_3$N$_4$ nanostructured flowers with superior photocatalytic hydrogen evolution performance. *ACS Appl. Mater. Interfaces* **2015**, *7*, 16850–16856. [CrossRef] [PubMed]

33. Han, C.; Ge, L.; Chen, C.; Li, Y.; Xiao, X.; Zhang, Y.; Guo, L. Novel visible light induced Co$_3$O$_4$-g-C$_3$N$_4$ heterojunction photocatalysts for efficient degradation of methyl orange. *Appl. Catal. B Environ.* **2014**, *147*, 546–553. [CrossRef]

34. Li, R.G.; Weng, Y.X.; Zhou, X.; Wang, X.L.; Mi, Y.; Chong, R.F.; Han, H.X.; Li, C. Achieving overall water splitting using titanium dioxide-based photocatalysts of different phases. *Energy Environ. Sci.* **2015**, *8*, 2377–2382. [CrossRef]

35. Miyoshi, A.; Nishioka, S.; Maeda, K. Water splitting on rutile TiO$_2$-based photocatalysts. *Chem. Eur. J.* **2018**, *24*, 18204–18219. [CrossRef] [PubMed]

36. Ibhadon, A.O.; Fitzpatrick, P. Heterogeneous photocatalysis: Recent advances and applications. *Catalysts* **2013**, *3*, 189–218. [CrossRef]

37. Ohtani, B. Titania photocatalysis beyond recombination: A critical review. *Catalysts* **2013**, *3*, 942–953. [CrossRef]

38. Kato, H.; Kudo, A. Water splitting into H$_2$ and O$_2$ on alkali tantalate photocatalysts ATaO$_3$ (A = Li, Na, and K). *J. Phys. Chem. B* **2001**, *105*, 4285–4292. [CrossRef]

39. Pan, C.; Jia, J.; Hu, X.; Fan, J.; Liu, E. *In situ* construction of g-C$_3$N$_4$/TiO$_2$ heterojunction films with enhanced photocatalytic activity over magnetic-driven rotating frame. *Appl. Surf. Sci.* **2018**, *430*, 283–292. [CrossRef]

40. Zhang, Y.; Heo, Y.J.; Lee, J.W.; Lee, J.H.; Bajgai, J.; Lee, K.J.; Park, S.J. Photocatalytic hydrogen evolution via water splitting: A short review. *Catalysts* **2018**, *8*, 655. [CrossRef]

41. Kumar, S.; Karthikeyan, S.; Lee, A. g-C$_3$N$_4$-based nanomaterials for visible light-driven photocatalysis. *Catalysts* **2018**, *8*, 74. [CrossRef]

42. Pant, B.; Park, M.; Park, S.J.; Kim, H.Y. One-pot synthesis of CdS sensitized TiO$_2$ decorated reduced graphene oxide nanosheets for the hydrolysis of ammonia-borane and the effective removal of organic pollutant from water. *Ceram. Int.* **2016**, *42*, 15247–15252. [CrossRef]

43. Ullah, R.; Dutta, J. Photocatalytic degradation of organic dyes with manganese-doped ZnO nanoparticles. *J. Hazard. Mater.* **2008**, *156*, 194–200. [CrossRef] [PubMed]

44. Yu, W.; Chen, J.; Shang, T.; Chen, L.; Gu, L.; Peng, T. Direct Z-scheme g-C$_3$N$_4$/WO$_3$ photocatalyst with atomically defined junction for H$_2$ production. *Appl. Catal. B Environ.* **2017**, *219*, 693–704. [CrossRef]

45. Seong, D.B.; Son, Y.R.; Park, S.-J. A study of reduced graphene oxide/leaf-shaped TiO$_2$ nanofibers for enhanced photocatalytic performance via electrospinning. *J. Solid State Chem.* **2018**, *266*, 196–204. [CrossRef]

46. Nasir, M.S.; Yang, G.; Ayub, I.; Wang, S.; Wang, L.; Wang, X.; Ramakarishna, S. Recent development in graphitic carbon nitride based photocatalysis for hydrogen generation. *Appl. Catal. B Environ.* **2019**, *257*, 117855. [CrossRef]

47. Mamba, G.; Mishra, A.K. Graphitic carbon nitride (g-C$_3$N$_4$) nanocomposites: A new and exciting generation of visible light driven photocatalysts for environmental pollution remediation. *Appl. Catal. B Environ.* **2016**, *198*, 347–377. [CrossRef]

48. Patnaik, S.; Martha, S.; Parida, K.M. An overview of the structural, textural and morphological modulations of g-C$_3$N$_4$ towards photocatalytic hydrogen production. *RSC Adv.* **2016**, *6*, 46929–46951. [CrossRef]

49. Zhang, Y.; Liu, J.; Wu, G.; Chen, W. Porous graphitic carbon nitride synthesized via direct polymerization of urea for efficient sunlight-driven photocatalytic hydrogen production. *Nanoscale* **2012**, *4*, 5300–5303. [CrossRef]

50. Fajrina, N.; Tahir, M. A critical review in strategies to improve photocatalytic water splitting towards hydrogen production. *Int. J. Hydrog. Energy* **2018**, *44*, 540–577. [CrossRef]

51. Tay, Q.; Kanhere, P.; Ng, C.F.; Chen, S.; Chakraborty, S.; Huan, A.C.H.; Chen, Z. Defect engineered g-C$_3$N$_4$ for efficient visible light photocatalytic hydrogen production. *Chem. Mater.* **2015**, *27*, 4930–4933. [CrossRef]

52. Chen, Y.; Lin, B.; Wang, H.; Yang, Y.; Zhu, H.; Yu, W.; Basset, J.M. Surface modification of g-C$_3$N$_4$ by hydrazine: Simple way for noble-metal free hydrogen evolution catalysts. *Chem. Eng. J.* **2016**, *286*, 339–346. [CrossRef]

53. Wang, L.; Wang, C.; Hu, X.; Xue, H.; Pang, H. Metal/graphitic carbon nitride composites: Synthesis, structures, and applications. *Chem.-Asian J.* **2016**, *11*, 3305–3328. [CrossRef] [PubMed]

54. Martha, S.; Nashim, A.; Parida, K.M. Facile synthesis of highly active g-C$_3$N$_4$ for efficient hydrogen production under visible light. *J. Mater. Chem. A* **2013**, *1*, 7816–7824. [CrossRef]

55. Reddy, K.R.; Reddy, C.V.; Nadagouda, M.N.; Shetti, N.P.; Jaesool, S.; Aminabhavi, T.M. Polymeric graphitic carbon nitride (g-C$_3$N$_4$)-based semiconducting nanostructured materials: Synthesis methods, properties and photocatalytic applications. *J. Environ. Manag.* **2019**, *238*, 25–40. [CrossRef] [PubMed]

56. Zhou, L.; Zhang, H.; Sun, H.; Liu, S.; Tade, M.O.; Wang, S.; Jin, W. Recent advances in non-metal modification of graphitic carbon nitride for photocatalysis: A historic review. *Catal. Sci. Technol.* **2016**, *6*, 7002–7023. [CrossRef]

57. Xiao, M.; Luo, B.; Wang, S.; Wang, L. Solar energy conversion on g-C$_3$N$_4$ photocatalyst: Light harvesting, charge separation, and surface kinetics. *J. Energy Chem.* **2018**, *27*, 1111–1123. [CrossRef]

58. Yang, H.M.; Park, S.J. Influence of mesopore distribution on photocatalytic behaviors of anatase TiO$_2$ spherical nanostructures. *J. Ind. Eng. Chem.* **2016**, *41*, 33–39. [CrossRef]

59. Han, Q.; Wang, B.; Gao, J.; Cheng, Z.; Zhao, Y.; Zhang, Z.; Qu, L. Atomically thin mesoporous nanomesh of graphitic C$_3$N$_4$ for high-efficiency photocatalytic hydrogen evolution. *ACS Nano* **2016**, *10*, 2745–2751. [CrossRef]

60. Zhang, J.; Chen, Y.; Wang, X. Two-dimensional covalent carbon nitride nanosheets: Synthesis, functionalization, and applications. *Energy Environ. Sci.* **2015**, *8*, 3092–3108. [CrossRef]

61. Jing, L.; Ong, W.J.; Zhang, R.; Pickwell-MacPherson, E.; Jimmy, C.Y. Graphitic carbon nitride nanosheet wrapped mesoporous titanium dioxide for enhanced photoelectrocatalytic water splitting. *Catal. Today* **2018**, *315*, 103–109. [CrossRef]

62. Zhao, Z.; Wang, X.; Shu, Z.; Zhou, J.; Li, T.; Wang, W.; Tan, Y. Facile preparation of hollow-nanosphere based mesoporous g-C$_3$N$_4$ for highly enhanced visible-light-driven photocatalytic hydrogen evolution. *Appl. Surf. Sci.* **2018**, *455*, 591–598. [CrossRef]

63. Low, J.; Yu, J.; Jaroniec, M.; Wageh, S.; Al-Ghamdi, A.A. Heterojunction photocatalysts. *Adv. Mater.* **2017**, *29*, 1601694. [CrossRef] [PubMed]

64. Dong, F.; Zhao, Z.; Xiong, T.; Ni, Z.; Zhang, W.; Sun, Y.; Ho, W.K. In situ construction of g-C$_3$N$_4$/g-C$_3$N$_4$ metal-free heterojunction for enhanced visible-light photocatalysis. *ACS Appl. Mater. Interfaces* **2013**, *5*, 11392–11401. [CrossRef] [PubMed]

65. Kim, T.W.; Park, M.; Kim, H.Y.; Park, S.J. Preparation of flower-like TiO_2 sphere/reduced graphene oxide composites for photocatalytic degradation of organic pollutants. *J. Solid State Chem.* **2016**, *239*, 91–98. [CrossRef]

66. Chai, B.; Peng, T.; Mao, J.; Li, K.; Zan, L. Graphitic carbon nitride (g-C_3N_4)–Pt-TiO_2 nanocomposite as an efficient photocatalyst for hydrogen production under visible light irradiation. *Phys. Chem. Chem. Phys.* **2012**, *14*, 16745–16752. [CrossRef] [PubMed]

67. Ismail, A.A.; Bahnemann, D.W. Photochemical splitting of water for hydrogen production by photocatalysis: A review. *Sol. Energy Mater. Sol. Cells* **2014**, *128*, 85–101. [CrossRef]

68. Villa, K.; Domènech, X.; Malato, S.; Maldonado, M.I.; Peral, J. Heterogeneous photocatalytic hydrogen generation in a solar pilot plant. *Int. J. Hydrog. Energy* **2013**, *38*, 12718–12724. [CrossRef]

69. Pant, B.; Park, M.; Kim, H.Y.; Park, S.J. Ag-ZnO photocatalyst anchored on carbon nanofibers: Synthesis, characterization, and photocatalytic activities. *Synth. Met.* **2016**, *220*, 533–537. [CrossRef]

70. Gholipour, M.R.; Dinh, C.-T.; Béland, F.; Do, T.-O. Nanocomposite heterojunctions as sunlight-driven photocatalysts for hydrogen production from water splitting. *Nanoscale* **2015**, *7*, 8187–8208. [CrossRef]

71. Xu, J.; Huo, F.; Zhao, Y.; Liu, Y.; Yang, Q.; Cheng, Y.; Min, S.; Jin, Z.; Xiang, Z. *In-situ* La doped Co_3O_4 as highly efficient photocatalyst for solar hydrogen generation. *Int. J. Hydrog. Energy* **2018**, *43*, 8674–8682. [CrossRef]

72. Samsudin, E.M.; Hamid, S.B.A. Effect of band gap engineering in anionic-doped TiO_2 photocatalyst. *Appl. Surf. Sci.* **2017**, *391*, 326–336. [CrossRef]

73. Zhou, L.; Wang, L.; Zhang, J.; Lei, J.; Liu, Y. The preparation, and applications of g-C_3N_4/TiO_2 heterojunction catalysts—A review. *Res. Chem. Intermed.* **2017**, *43*, 2081–2101. [CrossRef]

74. Cao, S.; Jiang, J.; Zhu, B.; Yu, J. Shape-dependent photocatalytic hydrogen evolution activity over a Pt nanoparticle coupled g-C_3N_4 photocatalyst. *Phys. Chem. Chem. Phys.* **2016**, *18*, 19457–19463. [CrossRef] [PubMed]

75. He, Y.; Wang, Y.; Zhang, L.; Teng, B.; Fan, M. High-efficiency conversion of CO_2 to fuel over ZnO/g-C_3N_4 photocatalyst. *Appl. Catal. B Environ.* **2015**, *168*, 1–8.

76. Zhang, Z.; Liu, K.; Feng, Z.; Bao, Y.; Dong, B. Hierarchical sheet-on-sheet $ZnIn_2S_4$/g-C_3N_4 heterostructure with highly efficient photocatalytic H_2 production based on photoinduced interfacial charge transfer. *Sci. Rep.* **2016**, *6*, 19221. [CrossRef] [PubMed]

77. Yuan, J.; Wen, J.; Zhong, Y.; Li, X.; Fang, Y.; Zhang, S.; Liu, W. Enhanced photocatalytic H_2 evolution over noble-metal-free NiS cocatalyst modified CdS nanorods/g-C_3N_4 heterojunctions. *J. Mater. Chem. A* **2015**, *3*, 18244–18255. [CrossRef]

78. Zhang, J.; Ma, Z. $Ag_6Mo_{10}O_{33}$/g-C_3N_4 1D-2D hybridized heterojunction as an efficient visible-light-driven photocatalyst. *Mol. Catal.* **2017**, *432*, 285–291. [CrossRef]

79. Tan, Y.; Shu, Z.; Zhou, J.; Li, T.; Wang, W.; Zhao, Z. One-step synthesis of nanostructured g-C_3N_4/TiO_2 composite for highly enhanced visible-light photocatalytic H_2 evolution. *Appl. Catal. B Environ.* **2018**, *230*, 260–268. [CrossRef]

80. Zhang, H.; Liu, F.; Wu, H.; Cao, X.; Sun, J.; Lei, W. *In situ* synthesis of g-C_3N_4/TiO_2 heterostructures with enhanced photocatalytic hydrogen evolution under visible light. *RSC Adv.* **2017**, *7*, 40327–40333. [CrossRef]

81. Shi, Y.; Chen, J.; Mao, Z.; Fahlman, B.D.; Wang, D. Construction of Z-scheme heterostructure with enhanced photocatalytic H_2 evolution for g-C_3N_4 nanosheets via loading porous silicon. *J. Catal.* **2017**, *356*, 22–31. [CrossRef]

82. Lam, S.M.; Sin, J.C.; Mohamed, A.R. A review on photocatalytic application of g-C_3N_4/semiconductor (CNS) nanocomposites towards the erasure of dyeing wastewater. *Mater. Sci. Semicond. Process.* **2016**, *47*, 62–84. [CrossRef]

83. Ren, Y.; Dong, Y.; Feng, Y.; Xu, J. Compositing two-dimensional materials with TiO_2 for photocatalysis. *Catalysts* **2018**, *8*, 590. [CrossRef]

84. Li, Z.; Kong, C.; Lu, G. Visible photocatalytic water splitting and photocatalytic two-electron oxygen formation over Cu-and Fe-doped g-C_3N_4. *J. Phys. Chem. C* **2015**, *120*, 56–63. [CrossRef]

85. Iqbal, W.; Yang, B.; Zhao, X.; Rauf, M.; Waqas, M.; Gong, Y.; Mao, Y. Controllable synthesis of graphitic carbon nitride nanomaterials for solar energy conversion and environmental remediation: The road travelled and the way forward. *Catal. Sci. Technol.* **2018**, *8*, 4576–4599. [CrossRef]

86. Guo, Q.; Zhang, Y.; Qiu, J.; Dong, G. Engineering the electronic structure and optical properties of g-C_3N_4 by non-metal ion doping. *J. Mater. Chem. C* **2016**, *4*, 6839–6847. [CrossRef]

87. Feng, J.; Zhang, D.; Zhou, H.; Pi, M.; Wang, X.; Chen, S. Coupling P nanostructures with P-doped g-C_3N_4 as efficient visible light photocatalysts for H_2 evolution and RhB degradation. *ACS Sustain. Chem. Eng.* **2018**, *6*, 6342–6349. [CrossRef]